Biosensors and Bioelectronics ■ (■■■■) ■■■–■■■

Contents lists available at ScienceDirect

Biosensors and Bioelectronics

journal homepage: www.elsevier.com/locate/bios

An electrochemiluminescence biosensor for endonuclease EcoRI detection

Yingjie Li [a,1], Yuqin Li [c,1], Yaoyu Wu [a], Fushen Lu [a], Yaowen Chen [b], Wenhua Gao [a,b,*]

[a] Department of Chemistry and Laboratory for Preparation and Application of Ordered Structural Materials of Guangdong Province, Shantou University, Shantou, Guangdong 515063, PR China
[b] Analysis & Testing Center, Shantou University, Shantou, Guangdong 515063, PR China
[c] Department of Pharmacy, Taishan Medicine College, Taian, Shandong 271016, PR China

ARTICLE INFO

Article history:
Received 22 November 2015
Received in revised form
11 January 2016
Accepted 28 January 2016

Keywords:
ECL
GNPs-graphene
Amplifier
Endonucleases
EcoRI
$Ru(bpy)_3^{2+}$

ABSTRACT

Endonucleases cleavage of DNA plays an important role in biological and medicinal chemistry. This work was going to develop a reliable and sensitive electrochemiluminescent (ECL) biosensor for detecting endonucleases by using gold nanoparticles graphene composite (GNPs-graphene) as a signal amplifier. Firstly, the GNPs and graphene were simultaneously deposited on the glassy carbon electrode (GCE) by cyclic voltammetry. Then a stem DNA was anchored on the surface of GCE. And with a modifying DNA introduced into the electrode by DNA assembly, a strong ECL signal was obtained. After a DNA modified with ferrocene assembly to the stem DNA, the ECL signal had a sharp decrease due to the quench effect of ferrocene to and the biosensor comes into being a "off" state. With the effect of endonuclease, the ECL signal had a recovery because of the ferrocene being released and the biosensor formed a "on" state. Moreover, the recovery of ECL signal was related to the concentration of endonucleases. Combining specific defined DNA and endonuclease, this method has a potential to detect different endonucleases. In this work, we took the EcoRI as an example to identify the feasibility of ECL biosensor in applying in sensitive detection of endonucleases using a GNPs-graphene signal amplifier. Under optimal condition, the proposed biosensor obtained a low limit of detection (LOD) 5.6×10^{-5} U mL^{-1}. And the stability, selectivity and reproducibility of the biosensor also were researched.

1. Introduction

Endonucleases, a family of nuclease that mainly exists in prokaryotic organisms, are known as "molecular scissors" with highly specific activity in cleaving the phosphodiester bond within DNA at defined positions (Ordinario et al., 2014). The endonucleases have been widely used in PCR assay, gene mapping, medicinal chemistry, enzymatic amplification technique and nanostructures/nanodevices fabrication (Nygen et al., 2005; Nakazato et al., 2006; Kanaras et al., 2007; Langhans and Palladino, 2009). Endonucleases play an important role in prokaryotic organisms with the principal function of protecting host genome against foreign DNA (Galburt and Stoddard, 2002). Therefore, they have been deemed to be important targets in the discoveries of antimicrobial and antiviral drugs (Baughaman et al., 2012; Clercq, 2006; Choi et al., 2003). Accordingly, sensitively and quantitatively assaying endonuclease is critical and useful in drug-development process and disease prevention.

Many works have been done on assaying endonucleases including high-performance liquid chromatography (HPLC), enzyme-linked immunosorben assay (ELISA), gel electrophoresis, fluorescence resonance energy transfer (FRET), fluorescence polarization and gold nanoparticle based colorimetric methods and so on (Alves et al., 1989; Ulubas and Ertunc, 2004; Agarkova et al., 2006; Qian et al., 2014; Huang et al., 2011). Even though those methods are able to detect endonucleases precisely, they exist many disadvantages including sophisticated instrumentations, complicate procedure, high-cost. Recently electrochemiluminescent (ECL) has been well developed in biosensor with both advantages of chemiluminescence and electrochemistry, such as low back-ground signal, being easily controlled and detection (Muzyka, 2014; Yao et al., 2013; Huang et al., 2015). Particularly, the ECL biosensor based on the quenching or enhancement of /TPrA ECL system have been extensively investigated such as the quenching mechanism of /TPrA ECL system by ferrocene and phenol (Miao and Bard, 2003; Wei and Wang, 2011; Xing et al., 2014; Gao et al., 2013a, 2013b). Besides the quenching effect of ferrocene to is better than other (Cao et al., 2006).

The development of ultrasensitive ECL DNA biosensor mainly contributed to the popular strategy of signal amplification. The use

* Corresponding author at: Department of Chemistry and Laboratory for Preparation and Application of Ordered Structural Materials of Guangdong Province, Shantou University, Shantou, Guangdong 515063, PR China.
E-mail address: whgao@stu.edu.cn (W. Gao).
[1] Both the authors contributed to the paper equally.

http://dx.doi.org/10.1016/j.bios.2016.01.082
0956-5663/

of nanomaterial as amplifiers has attracted special interesting in ECL biosensor design such as carbon nanotubes, graphene, gold nanoparticle, nanocomposites etc. (Bertoncello and Forster, 2009; Xu et al., 2011; Wang et al., 2011; Wang et al., 2012a, 2012b). Especially, graphene is a one-atom-thick layer of graphite with two linear bands crossing at the Dirac point. With excellent physical and chemical properties, large surface area and controllable electronic properties graphene has become a promising electrode material in constructing ECL biosensor (Meriga et al., 2015; Ma et al., 2014a, 2014b; Li et al., 2012).

Many methods have been proposed for graphene production, among which the chemical reduction of graphene oxide (GO) obtained from ultrasonic exfoliation of oxidized graphite is the most convenient way to yield large quantities of graphene sheets (Stankovich et al., 2007). However, the practical application of graphene are challenged by its irreversible agglomeration both in the drying state and in common solvents, which significantly reduces its effectiveness. Introducing metal nanoparticles was initially proposed in order to separate graphene sheets. While nowadays, it is well realized that the dispersion of metal nanoparticles on graphene sheets also potentially provides a new way to develop novel catalytic, magnetic, and electronic materials (Xu et al., 2008). Graphene-metal nanocomposite has also been used in ECL biosensor fabrication as a signal amplifier and get a good performance (Wang et al., 2012a, 2012b).

To our best known that few works have been done on assaying endonucleases using an ECL method. In this work, we employed gold nanoparticles-graphene composite (GNPs-graphene) as the ECL biosensor amplifier to detect endonucleases. As shown in Scheme 1, the GNPs and graphene were simultaneously deposited on the glassy carbon electrode (GCE) by cyclic voltammetry (CV). And then a well-designed stem A-DNA modified with thiol was introduced to the surface of electrode by stable Au–S interaction. Followed that a B-DNA modified with $Ru(bpy)_3^{2+}$ and a C-DNA modified with ferrocene were anchored on the surface by DNA self-assembly and the duplex strand, coming into being form A-DNA, B-DNA and C-DNA, would provide a position that the endonucleases can recognize. When the $Ru(bpy)_3^{2+}$ modifying B-DNA joint in the biosensor, a strong ECL signal will be obtained. Because of the quenching effect of ferrocene to $Ru(bpy)_3^{2+}$, the C-DNA modifying ferrocene will cause a signal "off" state. Endonucleases are known as "molecular scissors" with highly specific activity in cleaving the phosphodiester bond within DNA at defined positions. We well defined the A-DNA, B-DNA and C-DNA to make sure that the endonucleases only were cut down at the specific position and released the ferrocene. Under the effect of endonucleases the ferrocene was released and produced a signal "on" state with ECL signal recovery. Therefore the ECL intensity of the DNA biosensor generated a "switch on" mode, which rises with an increase of the concentration of endonucleases, whereby allowing the quantitative detection of endonucleases. This paper takes EcoRI for example to provide a versatile avenue for selective and sensitive detection of different endonucleases by designing different DNA sequence.

2. Experimental

2.1. Reagents

The DNA oligonucleotide sequences for this experiment are shown below:

A. DNA
5′-SH-$(CH_2)_6$-GGGGTTGGGGAAGGGTACG*A**GG*
AATTCC*GGGTTGGG*-3′
B. DNA: 5′-NH_2-$(CH_2)_6$-CCCTTCCCCAACCCC-3′
C. DNA: 5′-CCCAACCC**GGAATTCC**T-$(CH_2)_6$-NH_2-3′

All oligonucleotides were purchased from Shanghai Sangon Biotechnology Co. Ltd. (Shanghai, China). The underlining section of the stem A-DNA is complementary to the B-DNA and the italic bases are complementary to the C-DNA. The bold bases are the recognition sequence of EcoRI. The symbol "^" is the position that the endonuclease EcoRI can recognize. Cis-Bis-(2,2′-bipyridine)dichlororuthenium(II) dehydrate (cis-$Ru(bpy)_2Cl_2 \cdot 2H_2O$) were bought from Precious Metal Research Institution (Yunnan, China). 2-mercaptohexanol (MCH) was purchased from Sigma-Aldrich (St. Louis, MO, USA). Tripropylamine (TPrA), N-hydroxysuccinimide ester (NHS), tetrachloroanric (III) acid tetrahydrate [$HAuCl_4 \cdot 4H_2O$], N,N′-dicyclohexyl carbodiimide (DCC), N,N′-dimethlformamide (DMF) were obtained from Aladdin Chemical Reagent Co. Ltd. (Shanghai, China). Endonuclease (EcoRI, EcoRV, PstI, NotI, RsaI, NcoI) and buffer for enzyme reaction were got from Beyotime Biotechnology CO. Ltd. (Shanghai, China). Graphite flakes (325 mesh) was bought from XFNANO material Tech CO. Ltd. (Nan Jing, China). All other chemical not mentioned here were of analytical reagent grade and were used as received. Millipore Milli-Q water (18 MΩ cm) supplied by a Millipore Milli-Q water purification system (Bedford, MA USA) was used throughout. A concentration of 0.1 M phosphate buffer saline (PBS, pH 7.5, 0.1 M NaCl+0.1 M NaH_2PO_4/

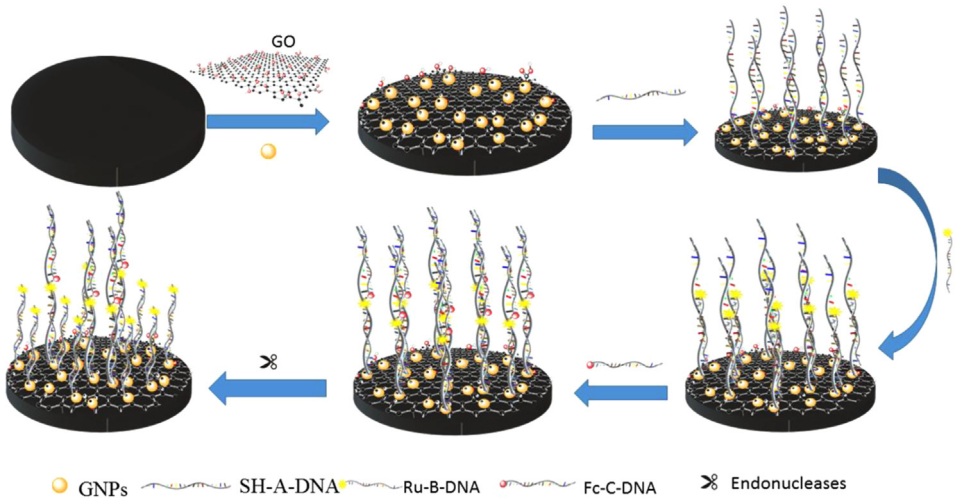

Scheme 1. Schematic diagram of the ECL biosensor for detection of endonucleases based on GNPs-graphene amplifier.

Na_2HPO_4) was used as hybridization buffer, binding buffer and washing solution. And a concentration of 50 mM Tris–HCl (pH 7.5, 10 mM $MgCl_2$, 100 mM NaCl, 0.02% Triton X-100, 0.1 mg/mL BSA) was used for enzyme reaction.

2.2. Apparatus

The ECL emission was detected with a computerized MPI-B type ultra-weak luminescence analyzer (Xi An Remax Electronic Science Tech. CO. Ltd. Xi An, China) equipped with a photomultiplier. The voltage of the photomultiplier tube (PMT) was set at −800 V. A conventional three-electrode system with a modified GCE (3 mm in diameter) used as a working electrode, a Ag/AgCl electrode as reference electrode and a platinum wire as auxiliary electrode. CV experiments and electrochemical impedance spectroscopy (EIS) were measured with an IM6ex electrochemical workstation (Zahner IM6ex, Germany). All measurements were carried out at room temperature. EIS was performed under an oscillation potential of 0.214 V over the frequency range of 1–100000 Hz. The electrochemical measurements were performed in the solution of 5 mM $[Fe(CN)_6]^{4-}$/$[Fe(CN)_6]^{3-}$ and 0.1 M KCl. Ultraviolet–visible (UV–vis) absorption spectra were recorded on a Lambda 950 spectrophotometer (Perkin Elmer, USA). Atomic force microscopy (AFM) image was got through tapping-mode on a Nanoscope IIIa Digital Instruments with NSC15 tips (Veeco, CA, USA). The morphologies of GNPs-graphene and graphene oxide were characterized by a scanning electron microscope (SEM, JSM-6360LA, JEOL, Japan), field emission scanning electron microscope (FE-SEM, XL30FEG, PHILIPS) and transmission electron microscope (FEI Tecnai F20 G2). X-ray diffraction (XRD) patterns was performed with a D8-Advance X-ray diffractometer (Bruker, Germany) operation using Cu Kα radiation. Raman spectra were recorded on a Jobin Yvon LABRAM-HR confocal laser micro-Raman spectrometer (Jobin Yvon, France) at a room temperature and an excitation wavelength of 514 nm.

2.3. The synthesis of biology beacon

Ruthenium bis(2,2′-bipyridine)-(2,2′-bipyridine-4,4′-dicarboxylic acid)-N-hydroxysuccinimide ester ([$Ru(bpy)_2$(debpy)NHS]) and the quenching probe ferrocene-labeled C-DNA (Fc-C-DNA) were synthesized according to our previous published paper. [$Ru(bpy)_2$(debpy)NHS] was directly used to mark the B-DNA to obtain the ECL probe of $Ru(bpy)_2$(dcbpy)NHS-B-DNA (abbreviated as Ru-B-DNA) (Gao et al., 2013a). The Ru-B-DNA was characterized by UV–vis spectroscopy to identify that $Ru(bpy)_2$(debpy)NHS was indeed labeled on the B-DNA (Fig. S1). The Fc-C-DNA was characterized through CV (Fig. S2). More details about the synthesis and characterization of Ru-A-DNA and Fc-C-DNA can be found in supplementary information.

2.4. Preparation of graphene oxide

Graphene oxide (GO) was prepared from graphite flakes (325 mesh) with a modified Hummer's method (Marcano et al., 2010). Concentrated H_2SO_4 (23 mL) was added to a mixture of graphite flakes (1 g) and $NaNO_3$ (0.5 g). And the mixture was cooled using an ice bath to 0 °C. $KMnO_4$ (3 g) was added slowly in portions to keep the reaction temperature below 20 °C. The reaction was warmed to 35 °C and stirred for 7 h. Additional $KMnO_4$ (3 g) was added in one portion, and the reaction was stirred for 12 h at 35 °C. The reaction mixture was cooled to room temperature and poured onto ice (~150 g) with 30% H_2O_2 (1 mL). The mixture was then purified following the protocol of sifting, filtering, centrifugation, decanting with multiple washes followed by a final vacuum drying to give the graphene oxide solid product.

2.5. The preparation of GNPs-graphene composite and fabrication of biosensor

GCE was polished with 0.3 and 0.05 μm α-Al_2O_3 slurry sequentially on a polishing cloth. The electrodes were fully rinsed after each polishing step and finally sonicated in deionized water and anhydrous ethanol for 5 min each, followed by electrochemical conditioning by potential scanning from −1 V to 1 V in 0.5 M H_2SO_4 for at least ten complete cycles at 100 mV s^{-1} until the reproducible cyclic voltammogram was obtained. Then the electrode was immediately used for deposition modification after a rinse step. The obtained GO powder was dispersed in a 0.07 M pH 8.0 phosphate buffer solution by ultrasonication to form a 1.0 mg mL^{-1} GO colloidal dispersion solution. The $HAuCl_4 \cdot 4H_2O$ was dissolved in the GO solution to form 100 μM $HAuCl_4$ solution. The GO and $HAuCl_4 \cdot 4H_2O$ can be simultaneously reduced on a GCE in 0.07 M pH 8.0 PBS solution by CV (Liu et al., 2011). The GNPs-graphene composite was obtained by CV from −1.5 V to 0.5 V at a scan rate of 10 mv s^{-1} for 10 cycles. Then, the GCE modified with GNPs-graphene composite was immersed in 5 μM A-DNA and stirred for 4 h at room temperature and then the electrode was incubated in 0.1 M PBS containing 1.0 mM 2-mercaptohexanol (MCH) for 20 min at room temperature. After a rising, the electrode was immersed into a 20 μL Ru-B-DNA solution for 2 h at 37 °C. At last, the electrode was immersed into a 20 μL Fc-C-DNA for 2 h at 37 °C and the biosensor for detection of EcoRI was obtained.

2.6. ECL measurements of the biosensor

The ECL biosensor was immersed in 200 μL of 50 mM Tis-HCl buffer containing different concentration of endonuclease EcoRI (10^{-4}, 10^{-3}, 10^{-2}, 10^{-1}, 1, 10, 20 U mL^{-1}), followed by a thorough washing with 0.1 M PBS solution to remove the released ferrocene, and then ECL measurements were carried out under scanning from 0.2 V to 1.25 V at 100 mV s^{-1} in 0.1 M PBS (pH 7.5, 0.1 M NaH_2PO_4/Na_2HPO_4+0.1 M NaCl) containing 0.1 M TPrA with a photomultiplier tube of −800 V. Quantification of target was based on the increment of ECL peak.

3. Results and discussion

3.1. Characterization of GO

Graphene oxide (GO) was synthesized from graphite by Hummers method, which was confirmed by AFM, FE-SEM, XRD respectively. The AFM image shows that the thickness of nanosheets was about 1 nm (Fig. 1A) and the lateral size was on the order of micrometers, which consistent with the precious literature (Marcano et al., 2010). Fig. 1B is the FE-SEM image of GO, and we can see many wrinkles on the surface of GO. The XRD patterns of natural graphite powder and exfoliated GO were recorded in Fig. 1C. Compared with natural graphite powder, the feature different diffraction peak of exfoliated GO appears at 10.28° (curve b), corresponding to reflection with a d-spacing of 0.894 nm, which is larger than natural graphite at 26.4° (curve a) (0.337 nm), indicating that the GO was obtained.

3.2. Characterization of GNPs-graphene composite and assembly electrode

The GNPs-graphene composite was got by simultaneously reducing GO and $HAuCl_4$ in PBS with CV from −1.5 V to 0.5 V at a scan rate of 10 mV s^{-1}. The GNPs-graphene was firstly characterized by CV and electrochemical impedance spectra (EIS) in 5 mM

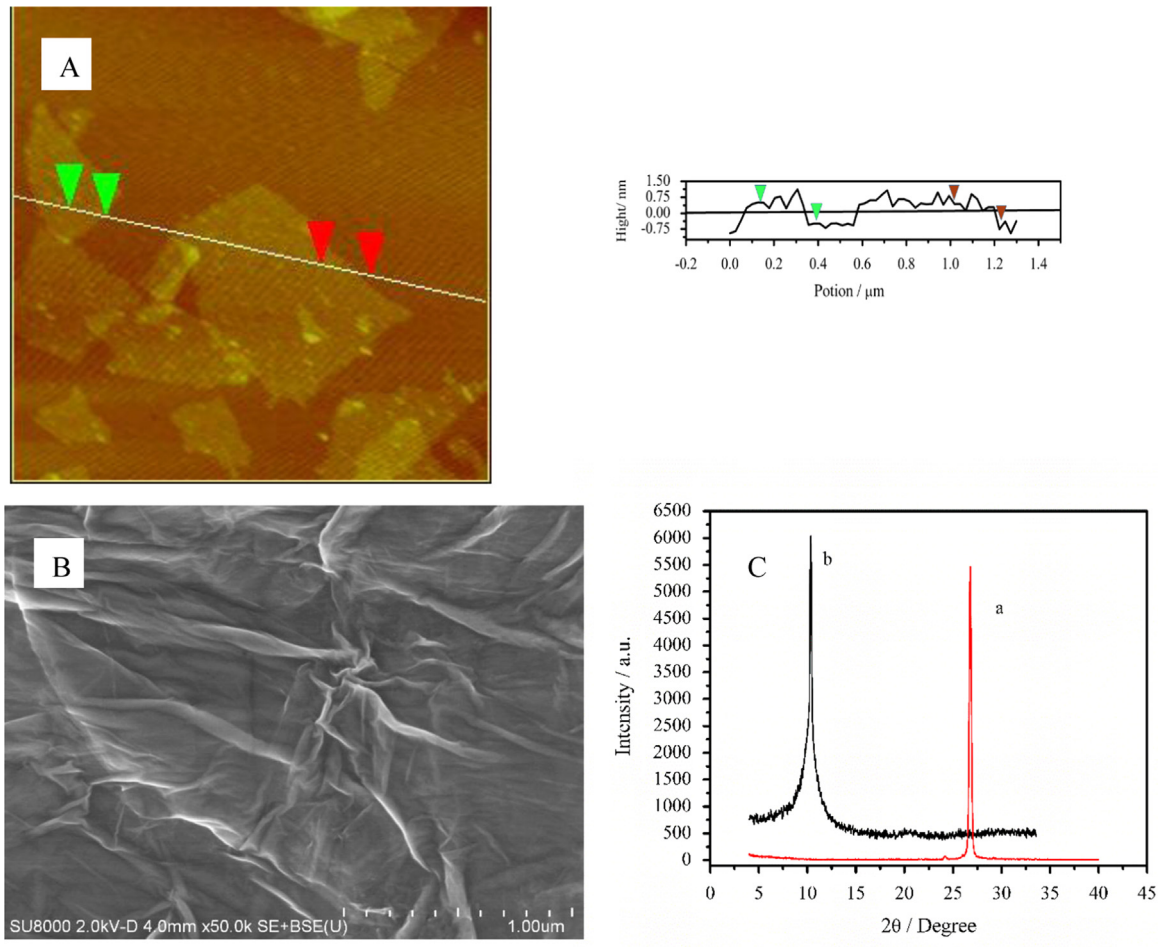

Fig. 1. (A) Tapping mode AFM of GO with height profiles deposited on freshly cleaved mica substrates; (B) FE-SEM image of GO; (C) XRD image of graphite (curve a) and GO (curve b).

$[Fe(CN)_6]^{4-}/[Fe(CN_6)]^{3-}$ containing 0.1 M KCl solution. Compared with the bare GCE, there is a big increase in current. In Fig. 2A, we can see the current of bare GCE is 1.0×10^{-4} A (curve a). And it changes to 1.4×10^{-4} A (curve b) after modifying. At last, the current decrease to 0.8×10^{-4} A (curve c) after A-DNA anchoring on GCE. The current of the electrode continued decreasing with B-DNA (curve d, 0.5×10^{-4} A) and C-DNA (curve e, 0.3×10^{-4} A) introducing the surface of the electrode. In the Nyquist diagram, the semicircle diameters at high frequency region reflect the electron transfer resistance (Ret) which related to the electron transfer resistance kinetics of the redox probe at electrode interface, and the linear part at lower frequencies corresponds to the diffusion resistance (Tang et al., 2010). The EIS was given in Fig. 2B. It is seen that the bare GCE exhibits a small semicircle with the Ret value at about 275 Ω (curve a). And the Ret is almost close to zero (curve b) after the GNP-graphene depositing on GCE. It means that the GNPs-graphene modifying GCE has a better electron transfer efficient. When the A-DNA was introduced to the surface of GCE, Ret increased (curve c) again due to the resistance of biomolecule to electron. The Ret continued increasing with B-DNA (curve d) and C-DNA (curve e) introducing to the surface of electrode. The SEM image of GNPs-graphene was given in Fig. 2C. It can be seen that the Au nanoparticles were uniformly dispersed on the reduced graphene.

As shown in Fig. 2D, Raman spectra of grapheme oxide (GO) (a), graphene (b), GNPs-graphene (c) were given. The Raman feature at 1352 cm^{-1}, known as the D band, arises from breathing of the hexagonal carbon ring due to the presence of defects. And another strong Raman feature observed at 1590 cm^{-1} is the E_{2g} mode (G band), assigned for the in-plane stretching of C–C bonds, which dictates the graphitic sp^2 crystalline nature of the carbon. We can see the G band of GO is little stronger than D band (curve a). The Raman spectrum of the reduced GO also contains both G and D bands (curve b); however, with an increased D/G intensity ration compare to that in GO. This change suggests a decrease in the average size of the sp^2 domains upon reduction of the GO, and can be explained if new graphitic domains were created that are smaller in size to the ones present in GO before reduction, but more numerous in number (Stankovich et al., 2007). The Raman spectra of GNPs-graphene (curve c) contains G and D bands too. Moreover the D/G intensity ration is close to the reduced GO and the intensity of D and G band have a striking enhancement. It may contribute to the charge transfer from Au to the grapheme and strong interaction between the Au and graphene layers (Biroju and Giri, 2014).

TEM and HRTEM were performed. As shown in Fig. 2E, we can see some gold nanoparticles spread on the graphene sheets. The size of the gold nanoparticles is about 2–8 nm. As shown in Fig. 2F, the distribution of GNPs on the graphene layers is further probed by HRTEM imaging. Bright and dark contrast regions represent the lattice patterns of the graphene without and with GNPs. The EDX was given in Fig. S3 and the outcome of the elements analysis is

Please cite this article as: Li, Y., et al., Biosensors and Bioelectronics (2016), http://dx.doi.org/10.1016/j.bios.2016.01.082

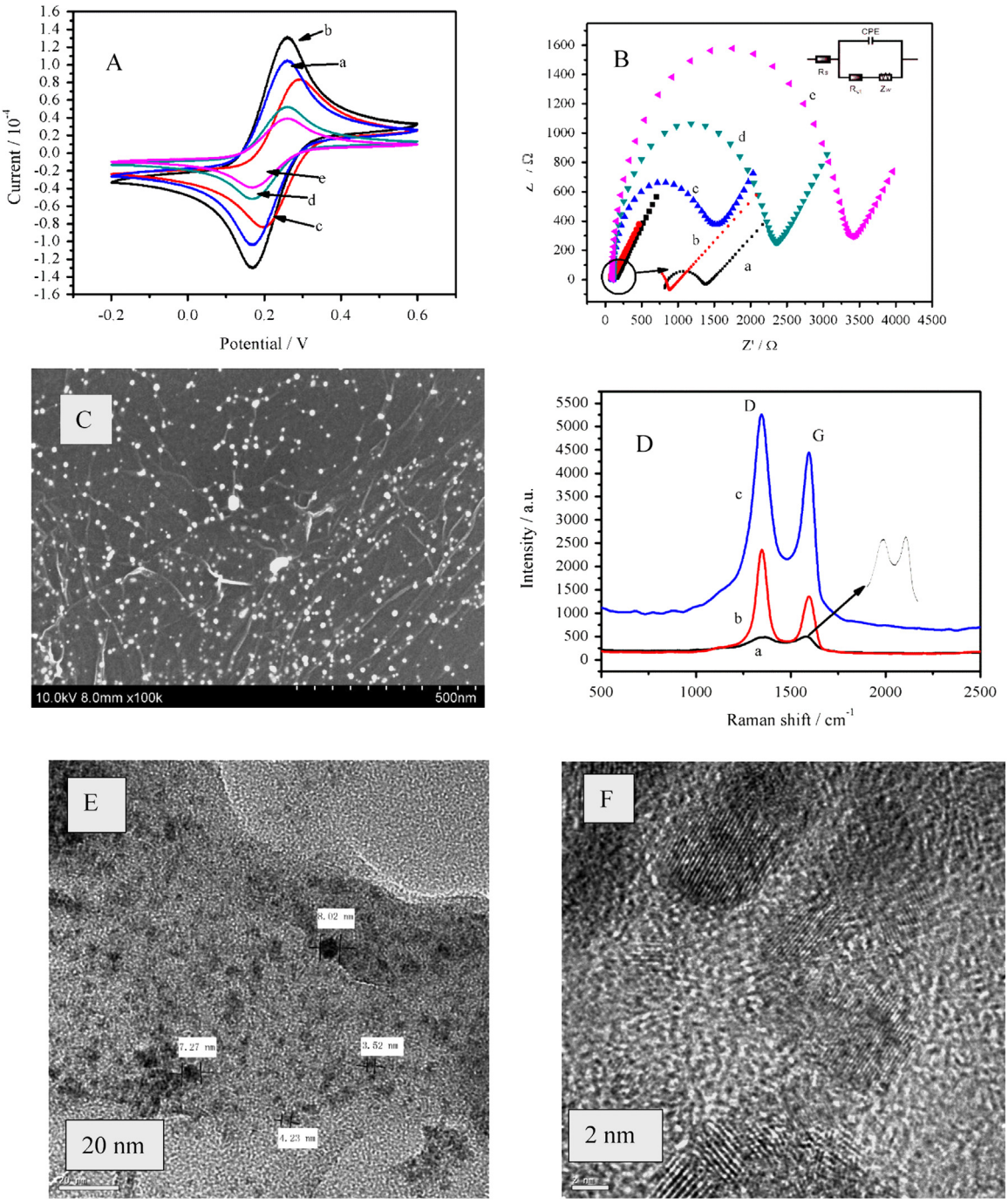

Fig. 2. (A) Cyclic voltammograms of different modified electrodes: (a) bare GCE, (b) GNPs-graphene modifying GCE, (c) A-DNA/GNPs-graphene modifying GCE, (d) A-DNA/B-DNA/GNPs-graphene modifying GCE, (e) A-DNA/B-DNA/C-DNA/GNPs-graphene modifying GCE in the solution of 5 mM $[Fe(CN)_6]^{4-}$/$[Fe(CN)_6]^{3-}$ containing 0.1 M KCl. Scan rate: 100 mV s^{-1}; (B) Nyquist diagram of electrochemical impedance spectra of different modified electrodes: (a) bare GCE, (b) GNPs-graphene modifying GCE, (c) A-DNA/GNPs-graphene modifying GCE, (d) A-DNA/B-DNA/GNPs-graphene modifying GCE, (e) A-DNA/B-DNA/C-DNA/GNPs-graphene modifying GCE. The inset of the top right corner is the equivalent circuit to fit with obtained EIS spectra, in the solution of 5 mM $[Fe(CN)_6]^{4-}$/$[Fe(CN)_6]^{3-}$ containing 0.1 M KCl; (C) the SEM images of GNPs-graphene; (D) the Raman spectrum of GO (a), RGO (b), GNPs-graphene (c); (E) and (F) the TEM images of GNPs-grapphene.

that C atom 88.92%, O atom 0.41%, Au atom 10.65% (atomic%).

To ensure the nanocomposite contains gold nanoparticles. The cyclic voltammetry of GNPs-graphene modifying GCE was measured in 0.05 M H_2SO_4. As shown in Fig. S4, curve a exhibited the bare GCE in 0.05 M H_2SO_4 solution without any obvious reversible peaks. After the electrodeposition of the GNPs-graphene on the surface of the GCE, curve b exhibited a reduction potential at 0.78 V and indicated that the nanocomposite contains gold nanoparticles (Hezard et al., 2012).

3.3. Incubation time of the biosensor electrode with EcoRI

As we known that the endonucleases can cleave the DNA at specific position, the sequence of DNA was cleaved to bring many active cohesive terminus. And those cohesive terminus can reconnect. In this work, the recovery of ECL signal rely on the release of ferrocene due to the function of endonucleases cutting the DNA. Therefore, long-time incubation may decrease the recovery of ECL signal and it is necessary

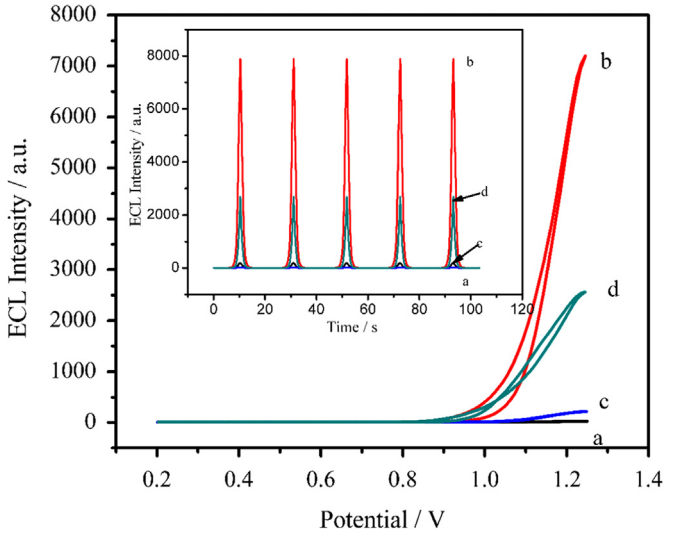

Fig. 3. ECL intensity vs. potential for (a) the A-DNA modified electrode, (b) A-DNA/Ru-B-DNA modified electrode, (c) A-DNA/Ru-B-DNA/Fc-C-DNA modified electrode, (d) the proposed biosensor after induction with EcoRI. Inset: ECL intensity vs. time curves for the biosensor under continuous CV for 5 cycles. ECL were measured in 0.1 M PBS containing 0.1 M TPrA at 100 mV s^{-1}.

to study the incubation time with EcoRI. In Fig. S5, it can get that the ECL intensity increased rapidly and reached a plateau after 30 min and decreased with more incubation. Therefore, 30 min is optimal incubation time with EcoRI for this experiment.

3.4. The stability of the GNPs-graphene composite as self-assembly platform

To explore the stability of the GNPs-graphene composite as self-assembly platform and its potential practicability in DNA hybridization ECL biosensor, A-DNA, Ru-B-DNA and Fc-C-DNA were introduced into the surface of the biosensor. The corresponding ECL signal of the biosensor electrode are presented in Fig. 3. As shown the Fig. 3, there is no obvious ECL signal response being found for the SH-A-DNA modified electrode (curve a). While the Ru-B-DNA was introduced into the system, a high signal was obtained (curve b). When Fc-C-DNA was assembled to A-DNA, the ECL decrease sharply (curve c) due to the quenching effect of ferrocene to $Ru(bpy)_3^{2+}$. There is an obvious increase of the ECL signal (curve d) after the proposed biosensor immersing in endonucleases for 30 min. Moreover, as shown in the inset of Fig. 3, continuous CV scanning the electrode can give an balanced ECL intensity which indicate that the SH-A-DNA, Ru-B-DNA and Fc-C-DNA can be stably attached to the GNPs-graphene without any molecules escaping from the electrode surface.

3.5. The stability, selectivity and reproducibility of the biosensor

The long-time stability of this endonuclease biosensor has been carried out. We can conclude from the result that the ECL response of the biosensor gradually decreased to approximately 96% of its original value after being stored in dark at 4 °C for one month (Fig. 4A). In addition, the ECL intensity of various concentration of EcoRI were further investigated. As shown in Fig. 4B, the ECL signal intensity increased with the increasing concentration of EcoRI. And a stable curve of different concentration could be obtained. These results demonstrated that the biosensor owned excellent stability.

To investigate the specificity of the biosensor, the ECL intensity was measured under same experimental condition after incubating with endonucleases EcoRV, PstI, NotI, RsaI and NcoI. As shown in Fig. S6, compared with the ECL response of biosensor to

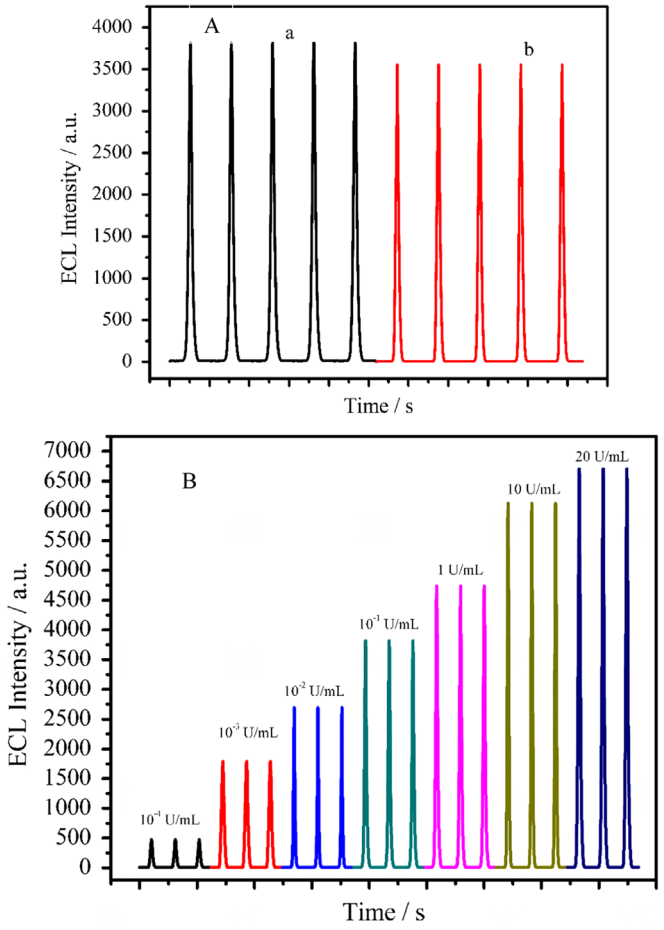

Fig. 4. (A) ECL intensity of the biosensor before and after one month in the presence of 0.1 U mL^{-1} EcoRI, (B) ECL stability of the proposed biosensor to various concentration of EcoRI. ECL were measured in 0.1 M PBS containing 0.1 M TPrA at 100 mV s^{-1}.

0.01 U mL^{-1} EcoRI, the biosensor has no significant response towards 10 U mL^{-1} EcoRV, PstI, NotI, RsaI and NcoI respectively. It suggested that above biosensor have a good selectivity to EcoRI.

The reproducibility of the proposed biosensor for endonuclease was assessed by the relative standard derivations (RSD). Which were evaluated by measuring one EcoRI level for 5 reduplicate measurements. The RSD obtained form 10^{-4}, 10^{-3}, 10^{-2}, 10^{-1}, 1, 10, 20 U mL^{-1} EcoRI were 8.4%, 4.2%, 3.8%, 4.7%, 5.2%, 7.3%, 9.3% respectively which indicate the biosensor have a good reproducibility.

3.6. Analytical performance of the biosensor to EcoRI

Under the optimal conditions, the analytical performance of the biosensor to EcoRI was assessed by measuring the dependence of ECL intensity (I_{ECL}) on the concentration of EcoRI. As the Fig. 5 shown, the ECL intensity was enhanced with increasing concentration of EcoRI. And the I_{ECL} was found to be logarithmically related to the concentration of EcoRI in the range from 10^{-4} to 20 U mL^{-1} (inset of Fig. 5). The regression equation is $I_{ECL} = 1109.42\ \lg C_{EcoRI} + 4914.10$ with a regression coefficient of 0.9987 and limit of detection (LOD) 5.6×10^{-5} U mL^{-1} which is defined as the concentration corresponding to the mean blank value plus 3 standard deviations. And the LOD is lower than other methods (Table S1). This result suggested the potential use of the proposed ECL biosensor for studies of endonuclease inhibition, drug-development process and disease prevention.

Please cite this article as: Li, Y., et al., Biosensors and Bioelectronics (2016), http://dx.doi.org/10.1016/j.bios.2016.01.082

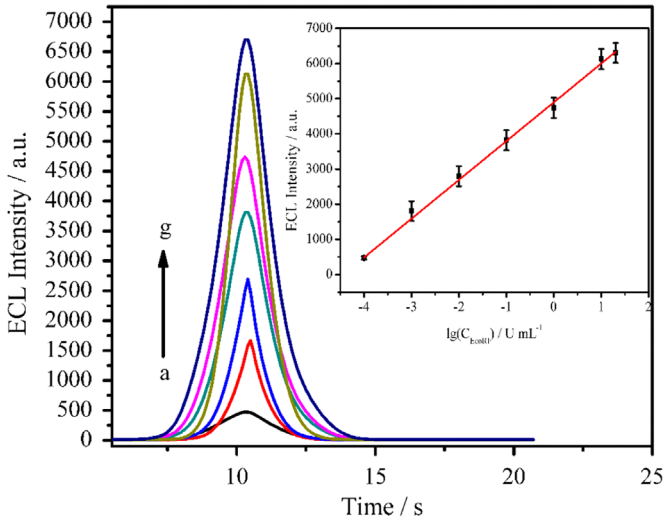

Fig. 5. ECL intensity of the biosensor with different concentration of EcoRI: (a) 10^{-4} U mL^{-1}, (b) 10^{-3} U mL^{-1}, (c) 10^{-2} U mL^{-1}, (d) 10^{-1} U mL^{-1}, (e) 1 U mL^{-1}, (f) 10 U mL^{-1}, (g) 20 U mL^{-1}. Inset: linear relationship between ECL intensity (I_{ECL}) and logarithm of the EcoRI concentrations. The error bars represent the standard deviation of three parallel measurements and ECL were measured in 0.1 M PBS containing 0.1 M TPrA at 100 mV s^{-1}.

3.7. Application of the biosensor in real samples

To study the applicability of the proposed biosensor in the practical samples, the assay was investigated to detect EcoRI in lake water. Firstly, 20 μL cell lysis solution was added into 20 μL lake water and the ECL intensity was measured. There is no obvious signal increasing with lake water. To further demonstrate the feasibility of biosensor in practical sample, the recovery experiments were performed and showed the acceptable data of the samples with recoveries between 94.0% and 105.6%. While the standard solutions recoveries were between 94.8% and 101.3%. The recoveries in 20 μL lake water given in table S2. Therefore, it suggests good accuracy of the proposed biosensor for real samples detection.

4. Conclusions

In summary, in this work, we have initiated to use an ECL biosensor for different endonucleases detection. We take the endonuclease EcoRI as an example to demonstrate this method feasibility to different endonucleases. Under optimal conditions, we explore the sensitivity of the biosensor and get a low LOD of 5.6×10^{-5} U mL^{-1} with a regression coefficient of 0.9987. The result demonstrated that our approach not only have the potential to provide a platform for detecting different endonucleases, but also may be used in studies of endonuclease inhibition, drug-development process and disease prevention.

Acknowledgements

We are grateful for the financial support from the Natural Science Foundation of Guangdong Province (Nos. S2011010005208 and 2014A030313480), the Guangdong High Education Fund of Science and Technology Innovation (No. 2013KJCX0078), the Science & Technology Project of Guangdong Province (No. 2013B030600001) and the National Natural Science Foundation of China (No. 51272152/E0208).

Appendix A. Supplementary material

Supplementary data associated with this article can be found in the online version at http://dx.doi.org/10.1016/j.bios.2016.01.082.

References

Agarkova, I.V., Dunigan, D.D., Van Etten, J.L., 2006. J. Virol. 80, 8114–8123.
Alves, J., Rulter, T., Geiger, R., Fliess, A., Maass, G., Pingoud, A., 1989. Biochemistry-US, 2678–2688.
Baughaman, B.M., Slavish, P.J., DuBois, R.M., Boy, V.A., White, S.W., Webb, T.R., 2012. ACS Chem. Biol. 7, 526–534.
Bertoncello, P., Forster, R.J., 2009. Biosens. Bioelectron. 24, 3191–3200.
Biroju, R.K., Giri, P.K., 2014. J. Phy. Chem. C 118, 13833–13843.
Cao, W., Ferrance, J.P., Demas, J., Landers, J.P., 2006. J. Am. Chem. Soc. 128, 7572–7578.
Clercq, E.D., 2006. Nat. Rev. Drug Discov. 5, 1015–1025.
Choi, S.Y., Chang, C.E., Kin, S.C., So, J.–S., 2003. Anaerobe 9, 277–280.
Galburt, E.A., Stoddard, B.L., 2002. Biochemistry 41, 13851–13860.
Gao, W., Zhang, A., Chen, Y., Chen, Z., Chen, Y., Lu, F., Chen, Z., 2013a. Biosens. Bioelectron. 49, 139–145.
Gao, W., Chen., Y., Xi, J., Lin, S., Chen, Y., Lin, Y., Chen, Z., 2013b. Biosens. Bioelectron. 41, 776–782.
Hezard, T., Fajerwerg., K., Evrard, D., Collière, V., Behra, P., Gros, P., 2012. J. Electroanal. Chem. 664, 46–52.
Huang, X., Li, Y., Zhang, X., Chen, Y., Gao, W., 2015. Analyst 140, 6015–6024.
Huang, Y., Zhao, S., Chen, Z.–F., Liu, Y.–C., Liang, H., 2011. Chem. Commun. 47, 4763–4765.
Kanaras, A.G., Wang, Z., Hussain, I., Brust, M., Cosstick, R., Bates, A.D., 2007. Small 3, 67–70.
Langhans, M.T., Palladino, M.J., 2009. Curr. Issues Mol. Biol. 11, 1–12.
Li, F., Feng, Y., Zhao, C., Li, P., Tang, B., 2012. Chem. Commun. 48, 127–129.
Liu, C., Wang, K., Luo, S., Tang, Y., Chen, L., 2011. Small 7, 1203–1206.
Ma, Y., Zhao, M., Cai, B., Wang, W., Ye, Z., Huang, J., 2014a. Biosens. Bioelectron. 59, 384–388.
Ma, L., Zhu, Z., Li, T., Wang, Z., 2014b. Biosens. Bioelectron. 52, 118–123.
Marcano, D.C., Kosynkin, D.V., Berlin, J.M., Sinitskii, A., Sun, Z., Slesarev, A., Alemany, L.B., Lu, W., Tour, J.M., 2010. ACS Nano 4, 4806–4814.
Meriga, V., Valligatla, S., Sundaresan, S., Cahill, C., Dhanak, V.R., Chakraborty, A.K., 2015. J. Appl. Polym. Sci. 45, 42766.
Miao, W., Bard, A.J., 2003. Anal. Chem. 75, 5825–5834.
Muzyka, K., 2014. Biosens. Bioelectron. 54, 393–407.
Nakazato, T., Jung, M.–K., Housworth, E.A., Rieseberg, L.H., Gastony, G.J., 2006. Genetics 173, 1585–1597.
Nygen, A.O.H., Ameziane, N., Duarte, H.M.B., Vijzelaar, R.N.C.P., Waisfisz, Q., Hess, C. J., Schouten, J.P., Errami, A., 2005. Nucleic Acids Res. 33 (14), e128.
Ordinario, D.D., Burke, A.M., Phan, L., Jocson, J.–M., wang, H., Dickson, M.N., Gorodetsky, A.A., 2014. Anal. Chem. 86, 8628–8633.
Qian, Y., Zhang, Y., Lu, L., Cai, Y., 2014. Biosens. Bioelectron. 51, 408–412.
Stankovich, S., Dikin, D.A., Piner, R.D., Kohlhaas, K.A., Kleinhammers, A., Jia, Y., Wu, Y., Nguyen, S.T., Ruoff, R.S., 2007. Carbon 45, 1558–1565.
Tang, L., Feng, H., Cheng, J., Li, J., 2010. Chem. Commun. 46, 5882–5884.
Ulubas, C., Ertunc, F., 2004. J. Phytopathol. 152, 498–502.
Wang, J., Shan, Y., Zhao, W.-W., Xu, J.-J., Chen, H.-Y., 2011. Anal. Chem. 83, 4004–4011.
Wang, J., Han, H., Jiang, X., Huang, L., Chen, L., Li, N., 2012a. Anal. Chem. 84, 4893–4899.
Wang, K., Guan, Q., Liu, Q., Liu, W., Cai, J., 2012b. Mater. Lett. 80, 4–49.
Wei, H., Wang, E., 2011. Luminescence 26, 77–85.
Xing, D., Zhou, X., Zhu, D., Liao, Y., Liu, W., Liu, H., Ma, Z., 2014. Nat. Proto 9, 1146–1159.
Xu, S., Liu, Y., Wang, T., Li, J., 2011. Anal. Chem. 83, 3817–3823.
Xu, C., Wang, X., Zhu, J., 2008. J. Phys. Chem. C 112, 19841–19845.
Yao, W., Wang, L., Wang, H., Zhang, X., Li, L., Zhang, N., Pan, L., Xing, N., 2013. Biosens. Bioelectron. 40, 356–361.